Contents lists available at ScienceDirect

Biosensors and Bioelectronics

journal homepage: www.elsevier.com/locate/bios

A portable low-cost long-term live-cell imaging platform for biomedical research and education

Maria P. Walzik [a], Verena Vollmar [a], Theresa Lachnit [a], Helmut Dietz [a], Susanne Haug [a], Holger Bachmann [a], Moritz Fath [a], Daniel Aschenbrenner [a], Sepideh Abolpour Mofrad [a,b], Oliver Friedrich [a,b], Daniel F. Gilbert [a,b,*]

[a] Institute of Medical Biotechnology, Friedrich-Alexander-Universität Erlangen-Nürnberg, Erlangen, Germany
[b] Erlangen Graduate School in Advanced Optical Technologies (SAOT), Friedrich-Alexander-Universität Erlangen-Nürnberg, Erlangen, Germany

ARTICLE INFO

ABSTRACT

Time-resolved visualization and analysis of slow dynamic processes in living cells has revolutionized many aspects of in vitro cellular studies. However, existing technology applied to time-resolved live-cell microscopy is often immobile, costly and requires a high level of skill to use and maintain. These factors limit its utility to field research and educational purposes. The recent availability of rapid prototyping technology makes it possible to quickly and easily engineer purpose-built alternatives to conventional research infrastructure which are low-cost and user-friendly. In this paper we describe the prototype of a fully automated low-cost, portable live-cell imaging system for time-resolved label-free visualization of dynamic processes in living cells. The device is light-weight (3.6 kg), small ($22 \times 22 \times 22$ cm) and extremely low-cost (< €1250). We demonstrate its potential for biomedical use by long-term imaging of recombinant HEK293 cells at varying culture conditions and validate its ability to generate time-resolved data of high quality allowing for analysis of time-dependent processes in living cells. While this work focusses on long-term imaging of mammalian cells, the presented technology could also be adapted for use with other biological specimen and provides a general example of rapidly prototyped low-cost biosensor technology for application in life sciences and education.

1. Introduction

All biological phenomena are dynamic. Understanding these phenomena requires continuous, i.e. time-resolved, observation. One of the most commonly applied techniques for assessing dynamic phenomena in living cells is long-term observation or imaging using specialized research microscopes (Terryn et al., 2009). Long-term imaging has been applied in a variety of fields of research including developmental biology (Heim et al., 2012; Morris and Spradling, 2011), histology (Pampaloni et al., 2013), neuroscience (Kotaleski and Blackwell, 2010; Loverde et al., 2011; Olbrich et al., 2013), immunology (Day et al., 2009; Zaretsky et al., 2012), physiology (Henke et al., 2013; Kim et al., 2008), functional genomics (Ganem et al., 2009; Harper et al., 2010; Neumann et al., 2006), stem cell (Endele and Schroeder, 2012; Kissa and Herbomel, 2010; Weber et al., 2013; Zhong et al., 2010) and cancer research

(Huang et al., 2011; Lv et al., 2012). Observed probes range from human and other mammalian culture (Weber et al., 2013), primary (Heim et al., 2012; Lv et al., 2012) and stem cells (Kotaleski and Blackwell, 2010; Morris and Spradling, 2011) or tissues (Gogolla et al., 2006; Kim and Davidson, 2013) over whole organisms including fish (Feng et al., 2012), fruit flies (Morris and Spradling, 2011), nematodes (Krajniak and Lu, 2010) and polyps (Peterson and Torii, 2012), to plant cells (Reiter et al., 2012) as well as further mono and multicellular cellular organisms.

Commercially available long-term live-cell imaging systems are usually equipped with two main components: an optical system for visualization of cells at the microscopic level and an incubator for culturing cells. The optical system is used to recurrently image cells for several hours, days or even weeks resulting in hundreds to thousands of images that are combined in a time-lapse video, visualizing dynamic processes that are otherwise invisible to the human eye. The incubator is capable of maintaining optimal conditions necessary for culturing cells, including temperature and carbon dioxide concentration as well as humidity of the atmosphere. Besides these components commercially available

research microscopes suitable to long-term life cell imaging are typically equipped with additional parts, such as a motorized stage for scanning a biological probe, exchangeable objectives and infrastructure allowing for fluorescence or luminescence microscopy. The broad range of accessories of these systems offer a vast spectrum of functions and applications but, at the same time, also limits the applicability and is disadvantageous for a number of reasons. First, due to the vast range of functions commercially available long-term imaging systems are mostly complicated to use and tie up highly skilled staff for application and maintenance. Second, conventional devices are often bulky and immobile. In the case that biological samples are cultured at different locations, the probes need to be transported to the microscope which can cause delays or in the worst case failure of a planned experiment, e.g. if suitable means of transportation do not exist or if the biological specimen are very sensitive, such as cultures of primary neurons exhibiting delicate neuronal networks. Third, due to the broad range of accessories conventional devices are typically cost intensive and not readily applicable to a broad range of laboratories, for biology studies in low-resource settings or for educational purposes, e.g. in primary or secondary schools or universities.

Despite the fact that there are a number of examples on low-cost, e.g. smartphone-based imaging technologies (Breslauer et al., 2009; Gallegos et al., 2013; Smith et al., 2011; Tseng et al., 2010) as well as miniaturized devices for culturing cell lines (Kim et al., 2009; Weltin et al., 2014) the combination of both technologies in a low-priced portable device has not been reported yet. Furthermore, the majority of the presented technologies require specialized and cost-intensive infrastructure for production as well as a high level of skill with regard to customization, i.e. adaptation and implementation with other than the described applications.

The emergence of rapid prototyping technology such as 3D-printing, open source microcontroller infrastructure and low cost consumer electronics, mechanics and robotics parts, also adopted by the 'Maker' movement, a culture of do-it-yourself product design (The DIY dilemma, 2013; Landrain et al., 2013; Seyfried et al., 2014), makes it possible to quickly and easily engineer light-weight, user-friendly devices of reduced cost and complexity.

To overcome the limitations of commercially available technology described above we aimed to develop a long-term live-cell imaging system based on a 'Makers' approach that is straightforward and easy to use, customizable, robust and of handy size to fit on any desk, low cost and affordable to a broad range of research labs and educational institutions and at the same time versatile and resource efficient. To this end we aimed to use off-the-shelf electronic components as well as 3D-desktop printing and low-cost open-source microcontroller architecture, both being more and more prominent in the development of scientific devices (D'Ausilio, 2012; Frame and Leach, 2014; Leeuw et al., 2013; Marzullo and Gage, 2012; Pineño, 2014; Schubert et al., 2013; Starosolski et al., 2014; Stokes et al., 2013; Wittbrodt et al., 2014). We further aimed to evaluate the device with regard to its optical characteristics, its applicability to scanning microscopy of large biological samples as well as to the stability of environmental conditions required for long-term imaging of mammalian cell lines. In order demonstrate the applicability of our device to biomedical research we intended to conduct a case study with mammalian cells and to compare data obtained with our system with data from a commercial high-end live-cell long-term imaging system.

2. Results

We have developed a low-cost portable live-cell imaging platform that is suitable for maintaining optimal culture conditions and parallel time-resolved imaging of mammalian cell lines. We describe the characteristics of the optical system and the growth chamber and we demonstrate the applicability for biomedical research by long-term imaging of recombinant HEK293[YFPI152L] cells at varying culture conditions. We compare time-resolved imaging data generated using our platform to data obtained using a commercially available high-end research microscope and validate its applicability for analysis of slow dynamic processes in living cells.

The device is made up of a microscope mounted on a motorized stage and an incubator for maintaining optimal culture conditions. The platform enables microscopic evaluation in bright and dark field and was constructed using 3D desktop printing and off-the-shelf components, including a webcam for the microscope, temperature, gas and humidity sensors for environment control and open-source Arduino microcontroller boards for hardware control and data acquisition. A software interface was developed using LabVIEW and LabVIEW interface for Arduino (see Section 4 for details). The device has the shape of a cube with a side length of 22 cm and a total weight of 3.6 kg. The total cost of the system is < €1250. The device is shown in Fig. 1. A detailed list of electronic parts is included in the supplements.

2.1. Characteristics of the optical system

As a first step toward assessing the optical characteristics of the webcam-based microscope we calculated the pixel size of the 2 megapixel CMOS sensor based on its outer dimensions ($\sim 3.4 \times 1.9$ mm) and the number of image pixel (1920×1080 pixel) and confirmed an estimated pixel spacing of 1.75 μm by measuring the pixel width using a conventional research microscope (data not shown). In a next step we imaged a *1951 USAF resolution test chart* in dark field illumination (see Fig. 2A, B), determined the pixel scale (~ 550 nm/pixel) and calculated field-of-view (385×385 μm for an image of 700×700 pixel) and magnification of the microscope (~ 3-fold). The images shown in Fig. 2A and B demonstrate the ability of the modified webcam to clearly resolve the smallest structure represented in the test chart (group 7, element 6, corresponding to 228 line pairs/mm or 2.19 μm). Since the resolving power of the microscope could not be finally clarified with the test target we subsequently imaged 500 nm beads in bright and dark field illumination (see Fig. 2C, D) as described in Section 4. For determination of the microscope's resolution limit we defined resolution as the full width at half maximum (FWHM) of the measured point spread function (PSF), which was 1.5 μm, a value that compares well with conventional research microscopes (e.g. with $10 \times$ Objective, NA 0.25). The resolution was obtained by averaging the FWHM of ten different beads recorded in the dark field. Fig. 2D illustrates the limitation of the microscope with regard to visualization of delicate structures of low contrast. However, in automated microscopy, bright field images are typically used to extract qualitative information only. Quantitative analysis is usually based on images exhibiting a high signal-to-noise ratio, e.g. from fluorescence microscopy, that in our case are generated from label-free dark field imaging.

2.2. Scanning microscopy of large biological probes

To evaluate whether our device is suitable for scanning of biological probes larger than the field-of-view of the microscope, we cultured HeLa cervix carcinoma cells in 34-mm dishes and stained the cells using haematoxylin and eosin (H&E) as described in Section 4. In a next step, cells were imaged in a meander-like pattern at 900 (30×30) overlapping locations and were subsequently stitched using FIJI software (Schindelin et al., 2012) and the plugin *Grid/Collection stitching* (Preibisch et al., 2009) (see
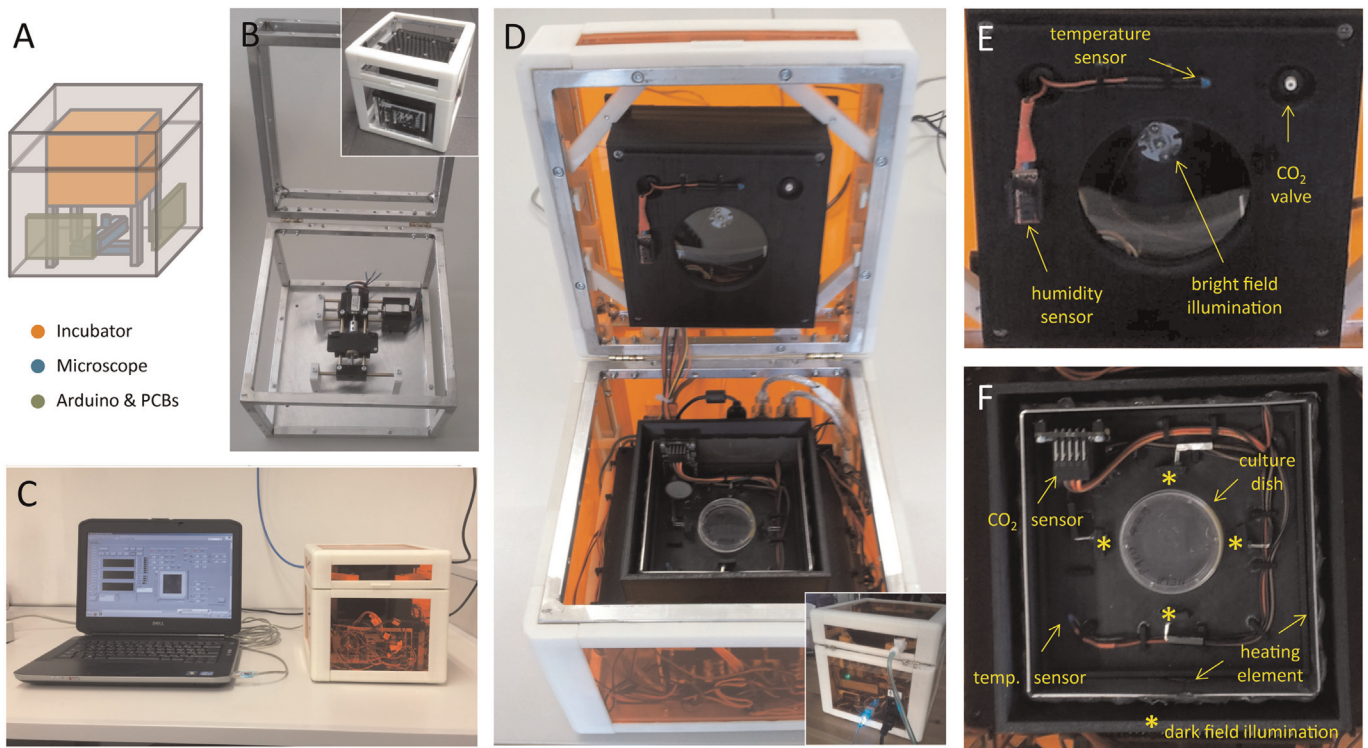
Fig. 1. The portable long-term live-cell imaging system is small (22 × 22 × 22 cm), light-weight (3.6 kg) and low-cost (< €1250). (A) Schematic drawing of the device and its main components. (B) Aluminium frame with mounted motorized stage but without microscope. In the fully assembled system, the microscope is mounted onto the black rectangular plane in the centre of the system. With a footprint of 12 × 12 cm (height: 7 cm), a scanning range of approx. 4 cm in x and y-direction, a resolution of 5 μm (± 5%) per step and material costs of around €300 including camera, motors, electronics, hard and software for automated and interactive control the fully assembled digital motorized microscope is extremely low-cost and compact at the same time. The inset shows the partly assembled system with 3D-printed parts (incubation chamber and housing) and a mounted PCB. (C) The device is controlled using a standard laptop computer and requires 220 V power and CO_2 gas supply but no additional equipment. CO_2 can be provided by either a laboratory gas line or a refillable gas container. (D) View into the interior of the incubator. The inset shows the rear view of the system with USB connection, CO_2 and power supply. (E) Enlarged view of the lid of the incubator. The lid is equipped with a white LED for bright field illumination, a gas valve as well as a heating element (not shown) to support homogeneous heat distribution inside the incubator. (F) Enlarged view of the incubator. The incubation chamber is equipped with sensors as indicated, with four cross-wise arranged white LED for dark field illumination as well as a heating element for temperature control. The platform is currently designed for application with 34-mm culture dishes that are placed over a circular hole at the base of the incubator allowing for microscopic evaluation of biological specimen.

Section 4). Fig. 3A shows the result of the reconstructed image. Enlarged image regions (white rectangles) of A, B and C are represented in B, C and D, respectively. These data demonstrate that our device allows automated scanning microscopy of large biological samples and visualization of single cells as well as delicate morphological features such as cellular extensions as highlighted by the white pointer in Fig. 3D.

2.3. Incubator characteristics

To assess the characteristics of the growth chamber with regard to the time period required for reaching equilibrium upon system start-up as well as the stability of culturing conditions during long-term operation, temperature and CO_2 concentration were set to standard conditions for mammalian cell lines (37 °C, 5% CO_2) and data of all sensors were recorded once every second for a total of 48 h. Prior to an experiment, a culture dish containing 3 ml culture media and a reservoir containing 10 ml deionized water was placed inside the incubator. Fig. 4 shows representative time-courses of temperature (A), CO_2 concentration (B) and relative humidity (C).

As indicated by the black arrow in Fig. 4A, the temperature inside the cell incubator reaches a steady-state oscillation around its set point of 37 °C (dotted line) approximately ten minutes after system start-up. The average amplitude and frequency of the oscillation (± SD), calculated from eleven independently and at ambient room temperature conducted experiments is 0.55 ± 0.05 °C and 0.003 Hz, respectively.

The CO_2 concentration quickly rises to a value of 6.8% after starting the system and subsequently declines with a slow rate to a sub-set point concentration of 4.8% followed by continuous oscillation around the set point of 5% (dotted line in Fig. 4B). As indicated by the black arrow, the steady-state oscillation is reached approx. 6 minutes upon system start-up. The average amplitude and frequency of the oscillation (± SD, n=11) is 1 ± 0.1% and 0.008 ± 0.001 Hz, respectively. At the given amplitude and frequency and an estimated incubator volume of 500 cm^3, the hourly CO_2 consumption of our device is ~150 ml.

Because humidification is achieved passively via evaporation from a water reservoir the humidity inside the incubator increases slowly and stabilizes at 70–80% after roughly two hours (black arrow in Fig. 4C).

These data show that the culture conditions reach equilibrium within a very short time upon system start-up and that our device does not require preparatory lead time.

Fig. 4D–F show mean values (± SD) of temperature, CO_2 and rel. humidity calculated from a 48 h period (with n=172,800 s or data points in a single experiment) from eleven independently conducted experiments each. The calculated mean values correspond well to the configured set points as well as to standard culturing conditions for mammalian cell lines. The overall low variability indicates that the culture conditions are stable within
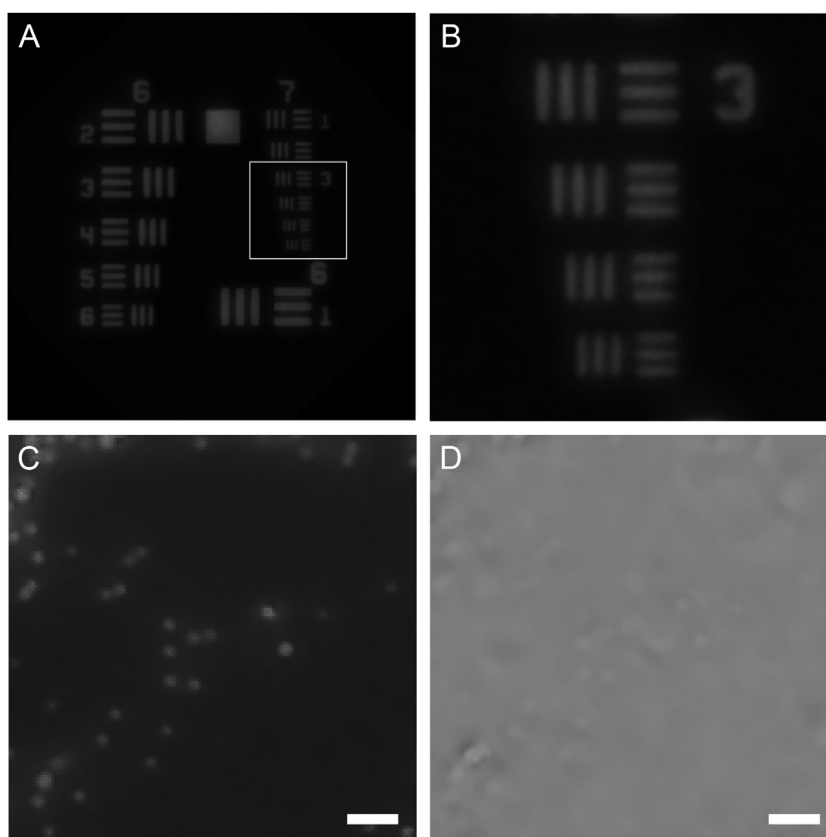
Fig. 2. The device is equipped with a webcam-based low-cost digital microscope generating images of a resolution comparable to conventional research microscopes. (A) USAF 1951 test target captured in dark field illumination. (B) Magnified representation of group 7, elements 3–6 from the image depicted in (A) illustrating the ability of the microscope to clearly resolve the smallest structure represented in the test chart (corresponding to a resolution of 2.19 μm). (C, D) Magnified representations of images of 500 nm latex beads recorded in dark and bright field illumination, respectively. The image in (C) was used for a conservative estimation of the microscope′s resolution limit, which was 1.5 μm, a value that compares well with conventional research microscopes, e.g. with $10 \times$ objective NA 0.25. Scale bar: 10 μm.

and between experiments and thus, demonstrate that our system is suitable for long-term operation.

2.4. Long-term live-cell imaging of mammalian cells

To prove that our platform is suitable for long-term parallel culture and imaging of mammalian cells we prepared HEK293[YFPI152L] cells as described in the methods section and kept cells in the system in Dulbecco′s modified Eagle′s medium (DMEM w/o phenol red) supplemented with 10% foetal calf serum and penicillin (100 U/ml)/streptomycin (100 mg/ml) for 48 h at 37 °C, 5% CO_2 and $> 70\%$ rel. humidity. Cells were imaged every 6 min in bright and dark field at 64 (8×8) overlapping locations. For visual inspection and quantitative image analysis the tiled images were stitched and spatially aligned using the ImageJ plugins *Grid/Collection stitching* and *Register Virtual Stack*, respectively. For quantitative image analysis, i.e. analysis of cell growth, the reconstructed and aligned dark field images were subsequently segmented using a modified version of the LabVIEW-based software DecTiff (Gilbert et al., 2009). Fig. 5 shows a gallery of bright and dark field, binary and overly images taken at 0, 6, 12, 18, 24, 30, 36, 42 and 48 h during the course of the experiment. A time-lapse video of the long-term live-cell imaging experiment can be found at https://vimeo.com/102333501.

These data show that our device allows fully automated time-resolved imaging and culture of mammalian cell lines. It enables visualization as well as quantification of slow dynamic processes that are otherwise invisible to the human eye.

2.5. Benchmarking with conventional technology

In order to demonstrate the applicability of the portable imaging system to biomedical research we measured the growth of HEK293[YFPI152L] cells at varying culture conditions using our device and compared these data to those generated with conventional technology (see Section 4). To this end we prepared HEK293[YFPI152L] cells as described in the methods section and kept cells for 48 h at 37 °C, 5% CO_2 and $> 70\%$ rel. humidity in Dulbecco′s modified Eagle′s medium (DMEM w/o phenol red) supplemented with penicillin (100 U/ml)/streptomycin (100 mg/ml) and varying concentrations of foetal calf serum (FCS). FCS promotes the growth of cells in a dose-dependent manner (Ryan, 1979). Mammalian cell lines are typically cultured in presence of 10–15% FCS. In order to establish varying culture conditions leading to attenuated, regular and accelerated cell growth we supplemented the culture media with 5, 15 and 25% FCS. Cells were imaged every 6 min in bright and dark field using the portable device and in fluorescence light using the reference system. For quantification of cell growth images were segmented and quantitatively analysed using a modified version of DecTiff software. Images generated by our device were stitched and spatially aligned prior to quantitative analysis. Fig. 6A and B show growth curves of HEK293[YFPI152L] cells (% of image area covered by cells) measured in presence of 5 (black), 15 (grey) and 25% (light grey) FCS using the low-cost platform (A) and the reference system (B), respectively. Data were averaged from three individual experiments (portable device) or three individual wells of a 384-well plate (reference system) each. Data acquired during the first 12 h of the experiment using the commercial long-term imaging system had to be omitted due to
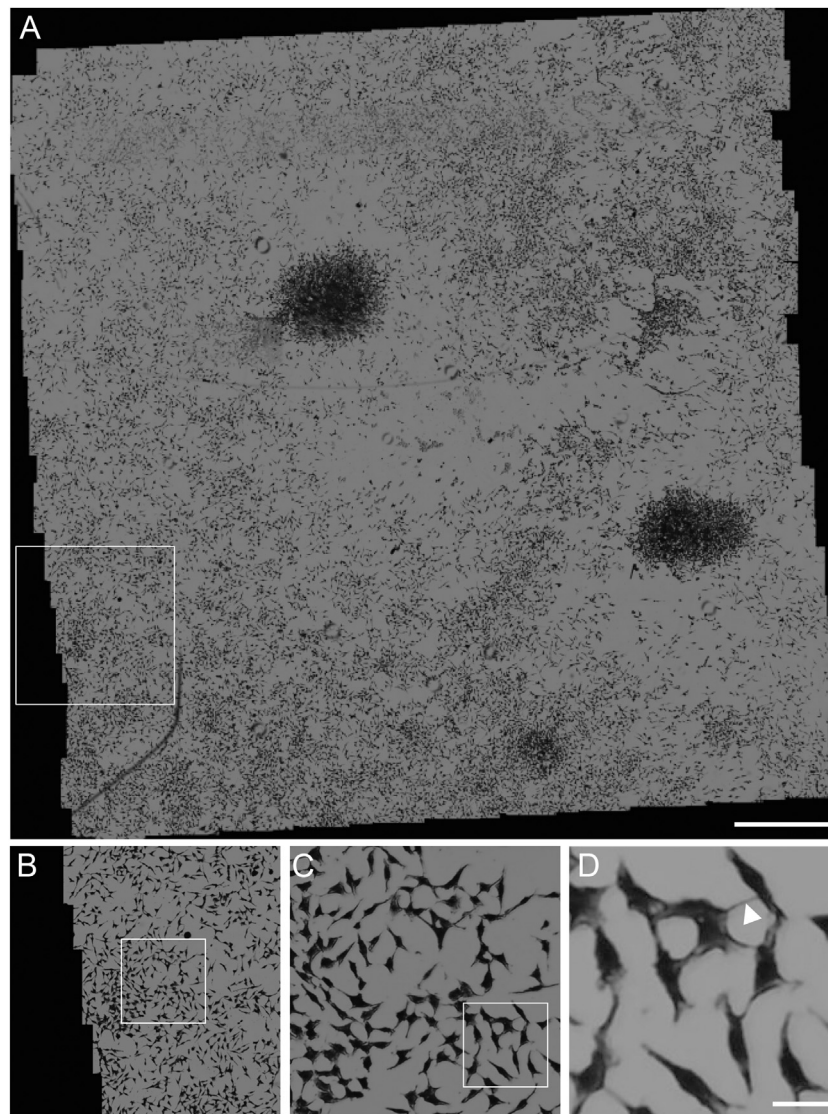
Fig. 3. A motorized stage allows scanning of biological specimen larger than the field-of-view of the microscope and visualization of subcellular structures. (A) Reconstructed bright field micrograph of H&E-stained HeLa cells imaged at 900 (30 × 30) overlapping locations. Enlarged image regions of (A), (B) and (C) are represented in (B), (C) and (D), respectively. The automated digital microscope generates images of high resolution suitable for visualization of single cells as well as delicate morphological features such as cellular extensions as highlighted by the white arrow in (D). Scale bars: (A) 500 μm, (D) 20 μm.

strong variation. Due to an inaccuracy of the microscope-stage of approximately ± 5% the imaging position varied between time points and resulted in stronger deviation of calculated growth area compared to conventional technology. As a quantitative measure for comparison of cell growth observed using our device and the reference system, we calculated the fold-change in growth area within a time period of 36 h from the experiments shown in Fig. 6A and B. Fig. 6C shows a correlation of the averaged fold-change in growth area observed in presence of different FCS concentrations calculated for the mobile technology and the reference system. The calculated mean values (± SD) are 1.15 ± 0.33, 2.07 ± 0.27 and 3.35 ± 0.93 as well as 0.13 ± 0.02, 1.97 ± 0.37 and 3.87 ± 0.18 for 5, 15 and 25% FCS for the low-cost platform and the high-end system, respectively.

Regression analysis (dashed lines) revealed excellent correlation with data from the classical approach (black, $R^2 = 0.99 \pm 0.22$). Thus, data generated in long-term live-cell imaging experiments using our platform compares well with data from conventional technology.

These results clearly demonstrate that the portable long-term live-cell imaging system is suitable to biomedical research.

3. Discussion

To overcome the limitations of commercially available technology suitable for long-term live-cell imaging we have developed a platform that is advantageous for several reasons. First, with a footprint of 22 × 22 cm and a mass of 3.6 kg the device is at least 10 times smaller and lighter compared to conventional technology allowing for mobile application. For operation the device requires 220 V power and CO_2 supply. CO_2 can be provided by either a laboratory gas line or a refillable gas container. The CO_2 consumption of around 150 ml/h accounts to a tenth of the hourly gas volume consumed by the reference system used in this study and supports the applicability of the presented technology as mobile device. Second, with < €1250 costs of material the portable device is 50–100 times less expensive compared to commercially available devices (e.g. Nikon Biostation IM-Q or the reference system used in this work) and is readily applicable to a broad range of laboratories in various fields of research and educational institutions. Third, the device was prototyped based on a 'Makers' approach, i.e. by using 3D desktop printing, off-the-shelf components and open-source microcontroller prototyping boards and
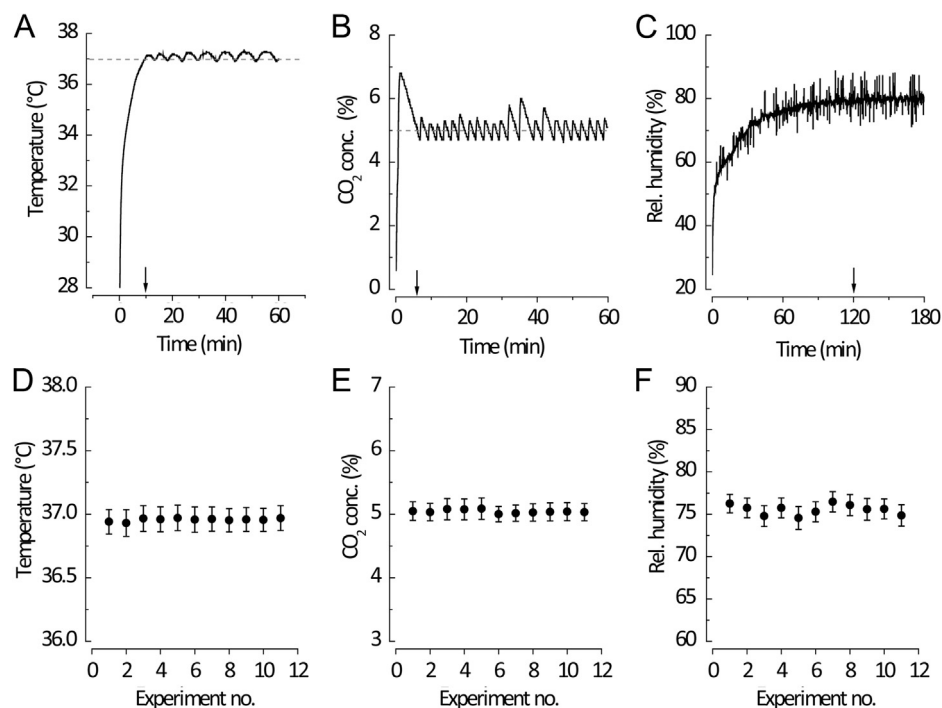
Fig. 4. The culture conditions in the growth chamber reach equilibrium shortly upon system start-up and are stable within and between individual long-term experiments. Representative time-courses of temperature, CO_2 concentration and rel. humidity within the growth chamber upon system start-up are shown in (A), (B) and (C). The arrows indicate time points at which optimal conditions were reached. Mean values ($\pm$ SD) of temperature, CO_2 and rel. humidity calculated from eleven independently conducted long-term-imaging experiments (48 h) are shown in (D), (E) and (F).
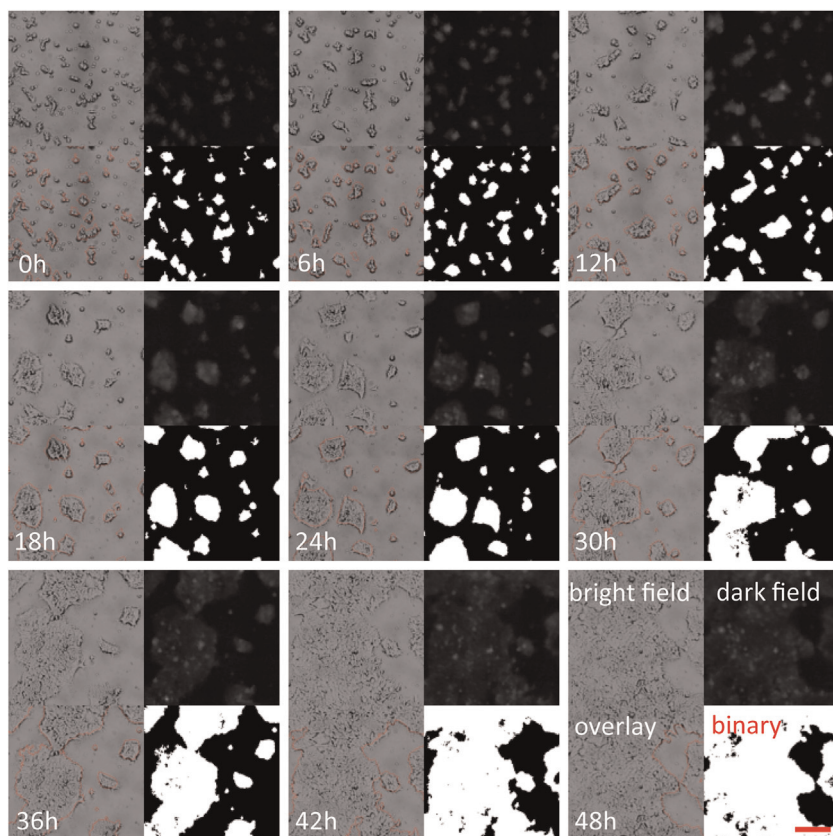

Fig. 5. The imaging platform is suitable to long-term live-cell imaging of mammalian cells at standard culture conditions. Bright field images (top-left in each box) were acquired for visual inspection and quality control. Dark field images (top-right in each box) facilitate image segmentation and quantitative analysis. Binary images (bottom-right in each box) are generated during image segmentation and were used for quantification of the image area covered by cells as well as for creation of overlay images (bottom-left in each box) that allow quality control of image segmentation. For space reasons, all images shown here were cropped from stitched and spatially aligned images. Link to the corresponding time-lapse video: https://vimeo.com/102333501 Scale bar: 50 μm.
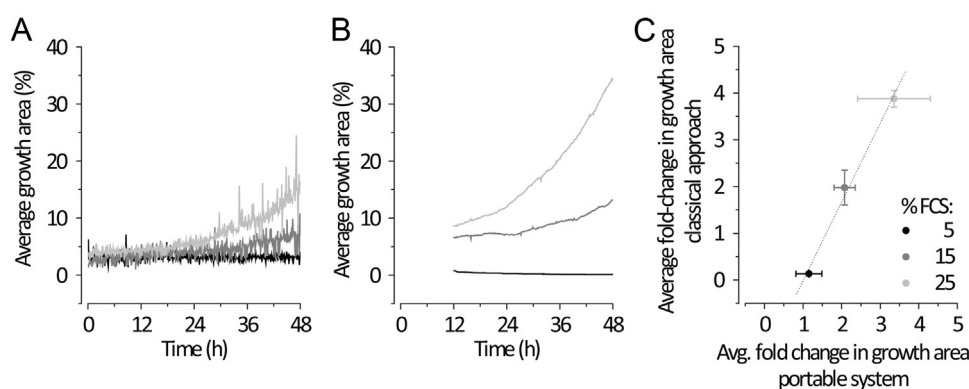
Fig. 6. Data recorded using the portable long-term life-cell imaging system compare well with data from conventional technology and demonstrate that the platform is suitable to biomedical research. Growth curves of HEK293^{YFPI152L} cells in presence of 5 (black), 15 (grey) and 25% FCS (light grey) measured using the portable device (A) and the reference system (B). (C) Correlation analysis of the average fold-change in growth area (in % of the image area) within a 36 h period in presence of varying FCS concentrations as shown in (A) and (B).

could easily be re-built or modified by individuals, e.g. in so called *fab labs* (fabrication laboratories), small-scale workshops which are increasingly being adopted by schools as platforms for project-based, hands-on STEM (science, technology, engineering and mathematics) education in an interdisciplinary and applied approach. 3D CAD files, schematics of PCBs or software code will be provided on request. Fourth, the device in its current configuration is straightforward, easy to use and does not require highly skilled staff for application and maintenance, further highlighting the applicability in the educational field.

The portable platform is equipped with a digital scanning microscope and light sources for imaging in bright and dark field at high resolution allowing for label-free time-resolved quantitative analysis of slow dynamic processes, such as proliferation, migration and morphogenesis in mammalian cell lines. When fluorescence indicators are to be used, the system could also be modified by implementation of excitation and emission filters as well as a dichroic filter and the appropriate light sources. With a footprint of 12×12 cm (height: 7 cm), and material costs of around €300 including camera, motors, electronics, hard and software for automated and interactive control, the motorized digital microscope is extremely small and at the same time cost-efficient. A range of approx. 4 cm in *x* and *y*-direction allows automated scanning of large biological specimen, such as cell cultures, tissues, organs and whole organisms as well as non-organic probes. In combination with e.g. custom designed multi-well sample carriers the stage enables operation in high-throughput format.

Although the system is currently set up for long-term parallel culture and imaging in 34-mm dishes it also enables automated microscopy with standard 26×76 mm glass slides (a 26×76 mm *USAF resolution test chart* was used for evaluation of the system's optical characteristics, see paragraph *Characteristics of the optical system*) and could be modified for application with 60-mm dishes within a short time and with little effort. However, larger standard culture formats, such as 100-mm dishes or multititer plates do not fit into the incubator and require the housing of the device to be re-designed.

A common issue in long-term lice-cell imaging is axial fluctuation, i.e. a focus drift during the course of the experiment. The phenomenon is predominately caused by thermal fluctuations (approx. one micron per degree Celsius) and gravity acting on the objective turret. Focus drift is progressively critical with increasing numerical aperture (NA), i.e. decreasing axial resolution of the used objective. For this reason, when high numerical aperture objectives are used in long-term live-cell imaging, additional infrastructure is required for keeping the biological probe in

focus. The estimated numerical aperture and axial resolution of the webcam-based microscope is approx. 0.2 and 35 μm, respectively, making the system less prone to fluctuations of the focal plane compared devices with objectives of high NA. Furthermore, the microscope is mounted onto a stage that is fixed in vertical direction and hence, not subjected to axial, e.g. gravitational forces. A time-lapse video of a long-term live-cell imaging experiment is provided at https://vimeo.com/102333501 demonstrating focus stability during long-term experimentation.

While software developed for the presented platform is mainly based on the programming language LabVIEW, system control and data acquisition could also be realized by other programming languages such as Arduino IDE, Linux, e.g. in conjunction with the novel prototyping platform Arduino Yún or μManager.

Although this work focusses on long-term imaging of mammalian cell lines, the presented technology could also be extended by implementation of further instrumentation including cooling infrastructure, liquid handling robotics or microfluidics, detectors allowing for monitoring of e.g. pH or metabolites as well as other biosensor technology to suit the requirements for a vast variety of fields of research including life and even material sciences.

In summary, the long-term live-cell imaging platform presented in this article improves the classical technologies in terms of portability, user-friendliness and cost and provides an example of low-cost biosensor technology that is compatible with fast and resource-efficient prototype optimization. Altogether, this work contributes to furthering the applicability and availability of commercially viable long-term live-cell imaging devices for use in biomedical research and education.

4. Methods

4.1. Housing

In total, more than 100 individual parts, including planes, brackets, pins, clamps, frames, spacers, blocks, etc. used for the cell incubation chamber, light sources, the microscope and motorized stage, the housing and other components were purpose-designed in CAD software (Autodesk Inventor 2013, Autodesk, Inc., USA) and manufactured from black and white acrylonitrile butadiene styrene (ABS, MakerBot Industries, USA) using a 3D printer (MakerBot Replicator, MakerBot Industries, USA). To ensure maximum mechanical stability at minimal weight – both essential for mobile use – the portable device is reinforced with a compact aluminium chassis (see Fig. 1B) enclosed by angled ABS profiles

and windows made of acrylic glass (Evonik Industries AG, Germany).

4.2. Incubator

4.2.1. Temperature control

The system is equipped with a total of 6 high precision thermistors (B+B Thermo-Technik GmbH, Germany) connected to a purpose-built sensor shield plugged on top of an Arduino Mega microcontroller board (Arduino, Italy). Four sensors are used for measuring and controlling temperature of the cell culture incubator of which two are installed close to the culture dish (beside and above, see Fig. 1F and G) and two sensors are mounted to the heating elements in the incubator and inside the lid of the incubator, respectively. The heating elements ensure optimal temperature distribution within the growth chamber. Both elements are made up of heating wire (16 Ω/m, Hinkel Elektronik, Germany) wrapped around either a frame of stainless steel (incubator) or four screws arranged in a square (lid). The heating elements are connected to a purpose-built actor shield plugged on top of an Arduino UNO microcontroller board (Arduino, Italy). Temperature is controlled by a software based feedback loop using the mean temperature reading of both sensors installed inside the incubator as actual value and a used-defined temperature as set point. Two sensors are used for monitoring ambient system and camera temperature. The analogue voltage read from the thermistor was translated to temperature (Kelvin) according to the Steinhart–Hart equation and was subsequently converted to degrees Celsius (°C) using the following equation:

$$T = \left(\frac{1}{(P + B) + (P^3 \times C) + A} \right) - 273.15$$

where T is the temperature in degrees Celsius (°C), A (1.129148×10^{-3}), B (2.34125×10^{-4}) and C (8.76741×10^{-8}) are Steinhart–Hart coefficients taken from the block diagram of the *Thermistor Read.vi* included in the LabVIEW Interface for Arduino toolkit. P is defined by

$$P = \left(\ln \left(\frac{R_{paired} \times V_{supply}}{V_{out}} \right) - R_{paired} \right)$$

R_{paired} is the value of a paired resistor (10,000 Ω). V_{supply} is the voltage provided by the power supply and V_{out} is the analogue voltage read from the thermistor.

4.2.2. CO$_2$ control

The CO_2 concentration in the incubation chamber is measured using a non-dispersive infrared (NDIR) absorption sensor (Gas Sensing Solutions Ltd., UK) mounted inside the incubator. Sensor readings are transmitted wirelessly using a wifi to RS232 UART adaptor module (Jinan USR IOT Technology Co.,Ltd., China). CO_2 is injected into the chamber with a solenoid valve (Respotec, Germany) installed in the lid of the incubator (see Fig. 1F) and connected the actor shield. The valve is triggered to open for 50 ms when the measured CO_2 concentration drops below a used-defined threshold. Gas pressure supplied by a laboratory gas line was set to 0.1 bar.

4.2.3. Humidity

Relative humidity inside the growth chamber is measured using a HIH-4030 humidity sensor (Honeywell, USA) plugged to the sensor shield. Humidification is achieved passively via evaporation from a printed 10 ml water reservoir placed inside the incubator. The analogue voltage read from the thermistor was translated to rel. humidity (%RH) using the following equation:

$$\%RH = \frac{\left(V_{out}/1023 \times V_{supply} \right) - Zero\ offset}{Slope}$$

where V_{out} is the analogue thermistor reading, V_{supply} is the supply voltage (5 V_{dc}), *Zero offset* is the analogue voltage measured at 25 °C, 0%RH and the supply voltage and *Slope* is the linear output of the thermistor measured during calibration at 25 °C and 5 V_{dc}. The values for *Zero offset* (0.0307) and *Slope* (0.958) were taken from the sensor′s datasheet.

Amplitude and frequency of temperature and CO_2 oscillations were analysed in LabVIEW.

4.3. Microscope

4.3.1. Construction

A low-cost webcam (Logitech, Switzerland) was modified to be used as a digital microscope. To this end, a purpose-designed plastic spacer was installed between the lens and the imaging chip. The objective of the unmodified webcam is designed to focus on distant objects with the lens being separated from the imaging chip by about the focal length. Increasing the distance between the objective and the image sensor by multiple focal lengths causes a magnified representation of the original object on the imaging chip. The size of the plastic spacer was determined empirically. The focal length of the optics was not characterized. Image distortion caused by spherical aberration in the optical system is handled by cropping the centre region (700 × 700 pixel) from the overall image (1920 × 1080 pixel) provided by the camera using LabVIEW 8.2 (National instruments, Ireland). The settings of the USB-connected camera, i.e. exposure time, brightness and contrast as well as the image acquisition rate are controlled in LabVIEW 8.2.

4.3.2. Resolution Limit

For determination of the microscope′s resolving power 0.5 µm beads (Life Technologies) were diluted 100-fold in deionized water and allowed to dry on a 34-mm culture dish. A series of one hundred images was acquired and was averaged using ImageJ for noise reduction.

4.4. Motorized stage

The microscope is mounted onto a custom-manufactured motorized stage made up of two orthogonally positioned bipolar step motors (200 Steps/Rev, NEMA 8, Watterott, Germany) each attached to a threaded spindle (1 mm pitch, Misumi, Japan) terminally centred using ball bearings (Kugellager Shop, Germany). The step motors are controlled via L293DNE H-bridge motor drivers (Texas Instruments, USA) mounted to the actor shield and software written in Arduino IDE and LabVIEW 8.2. To limit the travelling path of the stage each of the two axes is equipped with a pair of end switches (ZF Electronics, Germany) connected to the actor shield. The motorized stage allows imaging of probes larger than the field of view of the microscope in several tiled images but, due to an inaccuracy of approximately ± 5%, the generation of large reconstructed images requires post-acquisition image stitching of overlapping image tiles. The overlap was set to approximately 50% of the overall image dimensions.

5. Microcontroller boards

The whole system is orchestrated by two Arduino open-source electronics prototyping boards (Arduino, Italy) based on the ATmega328 (Arduino UNO) and the ATmega2560 (Arduino Mega

2560) microcontroller, respectively. The microcontroller on the boards was programmed using the Arduino open-source integrated development environment (IDE). The NI LabVIEW Interface for Arduino Toolkit (National Instruments, Ireland) was used for interfacing the Arduino boards with LabVIEW 8.2 through a serial connection.

5.1. Printed circuit boards

All electronic components, such as H-bridge motor drivers, low drop-out voltage regulators, capacitors, transistors, diodes, resistors, etc. are placed on two printed circuit boards (Fritzing Fab, Germany) purpose-designed in Fritzing 0.8.0 (Interaction Design Lab Potsdam, Germany). The circuit boards are Arduino-compatible and plug into the normally supplied Arduino pin-headers.

5.2. Power supply

The portable imaging system is fed with electricity from a 60 W open frame AC/DC triple output power supply (3.3/5/12 V, Top 60317, Traco Electronic AG, Switzerland).

5.3. Light sources

The portable platform is equipped with two different and individually controllable light sources allowing for imaging of biological probes in bright and dark field. Bright field illumination enables qualitative visual inspection of observed specimen but is not ideal for quantitative image analysis. Images obtained from label-independent dark field microscopy in turn are well-suited for quantitative and automated analysis due to their comparatively higher contrast. The light source for bright field imaging is realized with a LED (white light, EDEKA, Germany) mounted inside the lid of the incubator (Fig. 1F) opposite of the microscope. The light source for dark field illumination is made up of four crosswise arranged LEDs (white light, 3 mm, Nichia, Japan) located inside the growth chamber indirectly illuminating the probe (Fig. 1G).

5.4. Development process

The imaging platform was prototyped during a period of approx. 15 months, which can be divided into three phases. In the initial phase (6 months), the required electronic components were researched, ordered and assembled and preliminary circuits and software were developed. In the second phase (3 months) the motorized stage and the microscope were engineered, proof-of-concept experiments were carried out and a team for the final stage (6 months) was recruited. The team was composed of undergraduate students (Bachelor Programme *Life Science Engineering* at Friedrich Alexander University Erlangen-Nuremberg, Germany) who were involved in the development of printed circuit boards, the design of the device housing, system-assembly, software-customization, application with biological probes, benchmarking with conventional technology and local public relations.

5.5. User interface and data storage

A user interface for parametrization, calibration and application of the device, including camera settings, manual and automated control of the motorized stage, light sources, heating elements, the CO_2 solenoid valve, temperature and CO_2 gas set points, as well as for setting experimental parameters such as the number of image tiles, image acquisition rate and duration and data storage path are written in LabVIEW 8.2. The main VI is made up of 97 sub-Vis organized in 13 hierarchical levels. All recorded data are displayed online at the user interface and are saved at a frequency of 1 Hz in an ASCII-based log file allowing for post-experiment evaluation of the system's performance. Image data were digitized in 8-bit JPEG format to disk onto a laptop computer (Dell Latitude E5453, Dell, USA) with Windows 7 operating System (Microsoft Corporation, USA) but could also be replaced by any hand-held device running LabVIEW software.

5.6. Cell culture

All experiments were performed on recombinant HEK293[YFPI152L] cells cultured in Dulbecco's modified Eagle's medium (DMEM, Invitrogen) supplemented with 10% foetal calf serum and penicillin (100 U/ml)/streptomycin (100 mg/ml) (Sigma-Aldrich). Cells were cultured at 37 °C, 5% CO_2 in a humidified incubator according to standard procedures and were passaged weekly.

5.7. Cell lines

HEK293 and HeLa cervix carcinoma cells (CRL-1573™, CCL-2™) were purchased from *The American Type Culture Collection* (ATCC).

5.8. Haematoxylin and eosin staining

Haematoxylin and eosin staining of HeLa cervix carcinoma cells was done according to the manufacturer's instructions (Roth, Germany).

5.9. Generation of stable cell line

For generation of stable HEK293[YFPI152L] cell line, HEK293 cells were transduced with YFPI152L-expressing third generation lenti virus according to al Yacoub and collegues (al Yacoub et al., 2007). In brief, in a first step YFPI152L (Galietta et al., 2001) driven by the human polyubiquitin promoter C (hUbC) was subcloned into a pFUGW vector (Addgene). Third generation lenti viral packaging was done by calcium-phosphate transient transfection of HEK293 cells. For transfection, HEK293 cells were seeded into four T75 flasks (TPP, Switzerland) at 1×10^6 cells per flask in 10 ml of complete DMEM the day before transfection. One hour prior to transfection, the medium was replaced by 20 ml of new complete DMEM. For third generation packaging, 5.6 µg of transfer vector pFUGW-YFPI152L was mixed with 2.8 µg of pRRE (Addgene), 2.8 µg of pMD2 (Addgene), and 2.8 µg of pRSV-Rev (Addgene) helper plasmids. The mixture was diluted to a total volume of 2.4 ml in 2.5 M $CaCl_2$ (Sigma-Aldrich) and was added drop-wise to 2.4 ml of $2 \times$ BES-buffered saline (BBS, Sigma-Aldrich). Gentle mixing was then followed by a 12 min incubation period at room temperature. 1.6 ml of the plasmid mixture was added drop-wise to each cell flask and cells were returned to a lenti virus-allocated incubator and cultured at 37 °C and 3% CO_2 in a humidified atmosphere. Transfection mixture was removed three hours later, cells were washed five times with 10 ml PBS and 20 ml DMEM supplemented with 10 mM sodium butyrate (Sigma-Aldrich) were added per flask. 48 h later, the supernatant containing the final YFPI152L-expressing lenti virus was harvested and centrifuged at 1000 g for 10 min at 4 °C. The supernatant was then filtered through a 0.45 µm filter unit (Corning) and the filtrate was used for transduction. To this end, HEK293 cells were seeded into three T75 flasks at 1×10^6 cells per flask in 10 ml of complete DMEM the day before transduction. For transduction 5 ml of the medium was removed and 15 ml of the filtrate containing the virus harvest were added to the cells. 36-48 h later, virus media was removed from the cells and cells were washed five times with 10 ml PBS (Gibco). 10 ml of fresh media were added and cells were cultured for another 24 h at 37 °C, 5% CO_2 in a humidified incubator. Cells were then trypsinized with 0.25% Trypsin-EDTA (Sigma-Aldrich),

centrifuged at 300 g for 3 min at room temperature and washed with PBS before re-suspension in fresh media. Cells were subsequently grown in T75 flasks and the YFPI152$_L$-expressing cell population was enriched by fluorescence-activated cell sorting (MoFlo Legacy, Beckman Coulter). HEK293^{YFPI152L} cells were expanded in T75 flasks, cryo-conserved and used in long-term imaging experiments.

5.10. Preparation of cells for experiments

Approx. 1 h prior to commencement of experiments 3×10^5 and 4×10^3 cells suspended in 3 ml and 40 μl DMEM, supplemented with 5, 15 or 25% foetal calf serum and penicillin (100 U/ml)/streptomycin (100 mg/ml) were plated into 34-mm culture dishes and each well of a 384-well plate (BD Falcon) and were transferred to the portable device and the conventional high-end imaging system, respectively.

5.11. Long-term imaging experiments

5.11.1. Portable platform
The 34-mm culture dish was placed in the growth chamber and cells were cultured at 37 °C, 5% CO_2 and $> 70\%$ relative humidity and were imaged in bright and dark field every six minutes for at least 48 h in a grid of 64 (8×8) overlapping locations. In the current configuration scanning of a grid of 8×8 positions takes less than one minute.

5.11.2. Reference system
The 384-well plate was placed onto the motorized stage of a high-end long-term imaging system (Nikon Eclipse Ti, Nikon, Japan) equipped with a cell culture incubator with digital CO_2 controller (Okolab, Italy). Cells were cultured at 37 °C, 5% CO_2 and humidified atmosphere of unknown humidity and were imaged every six minutes with a 10x objective (CFI Plan Fluor DL 10 × Phase, N.A. 0.30, Nikon, Japan) for at least 48 h. Illumination from a xenon lamp (Lambda LS, Sutter Instruments, USA), passing through a filter block (C-FL Epi-FL FITC, EX 465-495, DM 505, BA 515-555, Olympus, Japan) was used to excite and detect YFP fluorescence signal. Fluorescence was imaged by a sCMOS camera (NEO, Andor, Ireland) and digitized to disk onto a personal computer (Dell Precision T3500, Dell, USA) with Windows 7 operating System (Microsoft Corporation, USA). The primary resolution of the camera was 2560×2160 pixel, although images were binned (2×2), resulting in a resolution of 1280×1080 pixel.

6. Image analysis

Images obtained from long-term imaging with our device were processed and quantitatively analysed using FIJI (ImageJ) and LabVIEW 8.2 software. In a first step, bright and dark field images from time-resolved tiled scans were stitched using the ImageJ plugin Grid/Collection stitching. In a next step the resulting reconstructed images were spatially aligned with ImageJ using the plugin Register Virtual Stack. The stitched and registered images obtained with the portable device as well as image data from the conventional high-end imaging system were quantitatively analysed using a modified version of DetecTiff software. In brief, dark field images were segmented using an iterative size and intensity-based thresholding algorithm and the area of identified cells was calculated as the percentage of the overall image size.

6.1. Data analysis

All calculations were done in Origin 7G (OriginLab Corporation, USA) if not stated otherwise.

6.1.1. Waveform analysis
Amplitude and frequency of temperature and CO_2 oscillations were analysed using LabVIEW 8.2.

6.1.2. Calculation of fold-change
As a quantitative measure for comparison of cell growth observed using our device and a high-end long-term imaging microscope we calculated the fold-change or increase of growth area within a time period of 36 h using the following equation:

$$Fold\ change = \frac{Area_{final}}{Area_{init}}$$

where $Area_{init}$ is the growth area observed after 12 h in culture and $Area_{final}$ is the image area covered by cells at the end of the experiment, i.e. 48 h in culture. $Area_{init}$ and $Area_{final}$ were obtained from individual growth curves upon applying a polynomial fit operation.

Author contributions

M.W., O.F. and Daniel F. Gilbert conceived the project and designed experiments. M.F. generated the stable cell line. V.V., H.D., S.H. and S.A.M. conducted experiments and analysed the data. T.L. and D.A. designed and printed 3D plastic parts. H.B. designed and assembled printed circuit boards and contributed to software development. M.W., O.F. and Daniel F. Gilbert wrote the paper.

Acknowledgements

Appendix A. Supplementary material

Supplementary data associated with this article can be found in the online version at http://dx.doi.org/10.1016/j.bios.2014.09.061.

References

Nature 503 (7477), 437–438.
al Yacoub, N., Romanowska, M., Haritonova, N., Foerster, J., 2007. J. Gene Med. 9 (7), 579–584.
Breslauer, D.N., Maamari, R.N., Switz, N.A., Lam, W.A., Fletcher, D.A., 2009. PLoS One 4 (7)e6320.
D'Ausilio, A., 2012. Behav. Res. Methods 44 (2), 305–313.
Day, D., Pham, K., Ludford-Menting, M.J., Oliaro, J., Izon, D., Russell, S.M., Gu, M., 2009. Immunol. Cell Biol. 87 (2), 154–158.
Endele, M., Schroeder, T., 2012. Ann. N. Y. Acad. Sci. 1266, 18–27.
Feng, Y., Renshaw, S., Martin, P., 2012. Curr. Biol. 22 (13), 1253–1259.
Frame, M., Leach, W., 2014. Surg. Technol. Int. 24, 314–318.
Galietta, L.J., Haggie, P.M., Verkman, A.S., 2001. FEBS Lett. 499 (3), 220–224.

Gallegos, D., Long, K.D., Yu, H., Clark, P.P., Lin, Y., George, S., Nath, P., Cunningham, B. T., 2013. Lab Chip 13 (11), 2124–2132.

Ganem, N.J., Godinho, S.A., Pellman, D., 2009. Nature 460 (7252), 278–282.

Gilbert, D.F., Meinhof, T., Pepperkok, R., Runz, H., 2009. J. Biomol. Screen. 14 (8), 944–955.

Gogolla, N., Galimberti, I., DePaola, V., Caroni, P., 2006. Nat. Protoc. 1 (3), 1223–1226.

Harper, C.V., Featherstone, K., Semprini, S., Friedrichsen, S., McNeilly, J., Paszek, P., Spiller, D.G., McNeilly, A.S., Mullins, J.J., Davis, J.R.E., White, M.R.H., 2010. J. Cell Sci. 123 (Pt 3), 424–430.

Heim, C.N., Fanslow, D.A., Dann, C.T., 2012. Biol. Reprod. 87 (4)90.

Henke, N., Albrecht, P., Bouchachia, I., Ryazantseva, M., Knoll, K., Lewerenz, J., Kaznacheyeva, E., Maher, P., Methner, A., 2013. Cell Death Dis. 4, e470.

Huang, Y., Hou, H., Yi, Q., Zhang, Y., Chen, D., Jiang, E., Xia, Y., Fenech, M., Shi, Q., 2011. DNA Repair 10 (6), 629–638.

Kim, H.M., Kim, B.R., An, M.J., Hong, J.H., Lee, K.J., Cho, B.R., 2008. Chemistry 14 (7), 2075–2083.

Kim, H.Y., Davidson, L.A., 2013. Cold Spring Harb. Protoc. 2013 (4), 366–369.

Kim, Y.-t., Karthikeyan, K., Chirvi, S., Davé, D.P., 2009. Lab Chip 9 (17), 2576–2581.

Kissa, K., Herbomel, P., 2010. Nature 464 (7285), 112–115.

Kotaleski, J.H., Blackwell, K.T., 2010. Nat. Rev. Neurosci. 11 (4), 239–251.

Krajniak, J., Lu, H., 2010. Lab Chip 10 (14), 1862–1868.

Landrain, T., Meyer, M., Perez, A.M., Sussan, R., 2013. Syst. Synth. Biol. 7 (3), 115–126.

Leeuw, T., Boss, E.S., Wright, D.L., 2013. Sensors, 13; , pp. 7872–7883.

Loverde, J.R., Ozoka, V.C., Aquino, R., Lin, L., Pfister, B.J., 2011. J. Neurotrauma 28 (11), 2389–2403.

Lv, L., Zhang, T., Yi, Q., Huang, Y., Wang, Z., Hou, H., Zhang, H., Zheng, W., Hao, Q., Guo, Z., Cooke, H.J., Shi, Q., 2012. Cell Cycle 11 (15), 2864–2875.

Marzullo, T.C., Gage, G.J., 2012. PLoS One 7 (3)e30837.

Morris, L.X., Spradling, A.C., 2011. Development 138 (11), 2207–2215.

Neumann, B., Held, M., Liebel, U., Erfle, H., Rogers, P., Pepperkok, R., Ellenberg, J., 2006. Nat. Methods 3 (5), 385–390.

Olbrich, L., Foehring, D., Happel, P., Brand-Saberi, B., Theiss, C., 2013. Histochem. Cell Biol. 139 (3), 431–445.

Pampaloni, F., Ansari, N., Stelzer, E.H.K., 2013. Cell Tissue Res. 352 (1), 161–177.

Peterson, K.M., Torii, K.U., 2012. J. Vis. Exp. 70.

Pineño, O., 2014. Behav. Res. Methods 46 (1), 196–205.

Preibisch, S., Saalfeld, S., Tomancak, P., 2009. Bioinformatics 25 (11), 1463–1465.

Reiter, S., Crescenzi, M., Galliot, B., Buzgariu, W., 2012. Int. J. Dev. Biol. 56 (6–8), 593–604.

Ryan, J.M., 1979. Effect of different fetal bovine serum concentrations on the replicative life span of cultured chick cells. In Vitro 15 (11), 895–899.

Schindelin, J., Arganda-Carreras, I., Frise, E., Kaynig, V., Longair, M., Pietzsch, T., Preibisch, S., Rueden, C., Saalfeld, S., Schmid, B., Tinevez, J.-Y., White, D.J., Hartenstein, V., Eliceiri, K., Tomancak, P., Cardona, A., 2012. Nat. Methods 9 (7), 676–682.

Schubert, T.W., D'Ausilio, A., Canto, R., 2013. Behav. Res. Methods 45 (4), 1332–1346.

Seyfried, G., Pei, L., Schmidt, M., 2014. Bioessays 36 (6), 548–551.

Smith, Z.J., Chu, K., Espenson, A.R., Rahimzadeh, M., Gryshuk, A., Molinaro, M., Dwyre, D.M., Lane, S., Matthews, D., Wachsmann-Hogiu, S., 2011. PLoS One 6 (3) e17150.

Starosolski, Z.A., Kan, J.H., Rosenfeld, S.D., Krishnamurthy, R., Annapragada, A., 2014. Pediatr. Radiol. 44 (2), 216–221.

Stokes, T.H., Venugopalan, J., Hubbard, E.N., Wang, M.D., 2013. Conf. Proc. IEEE Eng. Med. Biol. Soc. 2013, 2515–2518.

Terryn, C., Bonnomet, A., Cutrona, J., Coraux, C., Tournier, J.-M., Nawrocki-Raby, B., Polette, M., Birembaut, P., Zahm, J.-M., 2009. Crit. Rev. Oncol. Hematol. 69 (2), 144–152.

Tseng, D., Mudanyali, O., Oztoprak, C., Isikman, S.O., Sencan, I., Yaglidere, O., Ozcan, A., 2010. Lab Chip 10 (14), 1787–1792.

Weber, S., Fernández-Cachón, M.L., Nascimento, J.M., Knauer, S., Offermann, B., Murphy, R.F., Boerries, M., Busch, H., 2013. PLoS One 8 (2)e56690.

Weltin, A., Slotwinski, K., Kieninger, J., Moser, I., Jobst, G., Wego, M., Ehret, R., Urban, G.A., 2014. Lab Chip 14 (1), 138–146.

Wittbrodt, J.N., Liebel, U., Gehrig, J., 2014. BMC Biotechnol. 14, 36.

Zaretsky, I., Polonsky, M., Shifrut, E., Reich-Zeliger, S., Antebi, Y., Aidelberg, G., Waysbort, N., Friedman, N., 2012. Lab Chip 12 (23), 5007–5015.

Zhong, J.F., Weiner, L., Jin, Y., Lu, W., Taylor, C.R., 2010. Stem Cells Dev. 19 (1), 47–52.